Applications of femtosecond pulses for material investigations

Emil Eskol Svenningsen,* Mikkel Rasmussen,† and Nicolai R. Neubert‡

(Dated: March 24, 2025)

This report covers work done under the "Femtosecond Laser Pulse" project in relation to the "Large Experimental Exercises" course. During this project, we have worked with characterization of a femtosecond laser pulse duration and shape using the frequency-resolved optical gating (FROG) technique. We have also seen how femtosecond lasers can be used to study both generation of THz light from semiconductor surfaces and nonlinear fluorescence quenching.

I. INTRODUCTION

In this report, two applications of femtosecond (fs) laser pulses for material investigations are presented. These include *terahertz generation from semiconductor surfaces* and *nonlinear florescence quenching*. In addition, we also discuss *frequency-resolved optical gating* (FROG) as a method for characterizing the fs laser pulse.

Various techniques can be employed to generate THz radiation, one of these being the emerging field of 'Terahertz emission spectroscopy' (TES). This technique captures the ultrafast optical response of the materials upon illumination of fs laser pulses [1]. Because THz radiation is transparent for many materials (with metals and semiconductors being notable exceptions) and non-ionizing, it has several applications. For example, it can be used as a noncontact and nondestructive tool for probing semiconductor materials.

Using scintillator materials for the detection of highly energetic radiation can suffer from nonlinear quenching, decreasing the efficiency of the detector. In order to evaluate the quality of a material, one could probe these nonlinear effects using highly intense laser pulses.

II. THEORETICAL BACKGROUND

A. Terahertz generation from semiconductor surfaces using femtosecond lasers

Generation of terahertz (THz) radiation from the drift current arises as the time derivative of the photocurrent. In this case, initial carrier number and electron velocity before illumination are ignored. Relating the dipole moment, p, to the electric field of the generated radiation, E_{THz}, is typically done as

$$E_{\mathrm{Thz}} \propto \frac{\mathrm{d}^2 p}{\mathrm{d}t^2} \sin(\theta), \tag{1}$$

where θ denotes the angle between the dipole moment and direction of observation. By expressing the dipole moment in integral form using the charge density, $\rho(r)$, together with the continuity equation it is possible to show that $J = \mathrm{d}p/\mathrm{d}t$, and hence that

$$E_{\mathrm{Thz}} \propto \frac{\mathrm{d}J}{\mathrm{d}t}. \tag{2}$$

Achieving this experimentally can be done by irradiating a semiconductor with a femtosecond laser pulse, provided the photon energy is larger than the energy bandgap. In generating THz waves, there are two major mechanisms at play. Firstly, because the photocarriers are accelerated by a built-in field, a photocurrent will be generated, called a *drift current*. Secondly, these carriers may diffuse from the surface and into the material. Due to the mobility difference of electrons and holes a transient current is induced, called the *photo-Dember effect*. For normal semiconductors, such as GaAs, Si or InP, the driftcurrent is the dominant mechanism, whereas for narrow bandgap materials the diffusion dominates [1]. In the following these mechanisms are discussed in more detail.

Starting with the drift current, we rewrite eq. (2) using finite differences and using the fact that the current density $J = neV_d$,

$$J \propto \frac{\Delta n \Delta v}{\Delta t}. \tag{3}$$

Each of these can be expressed in terms of their respective proportionalities. For example, the carrier density, Δn, must be proportional to the pulse intensity, I_p, since each absorbed photon excited an electron-hole pair and the number of absorbed photons scales with I_p. In addition, the carrier acceleration, $\Delta v/\Delta t$, must be proportional to the (carrier)

* ess@phys.au.dk
† 202104473@post.au.dk
‡ neubert@au.dk

mobility, μ, and built-in electric field, E_B, since the carrier velocity goes as $v = \mu E_B$. Hence, in a simplified scheme the generated THz radiation can be understood from

$$E_{\mathrm{THz}} \propto \mu E_B I_p. \tag{4}$$

To refine this and account for depletion layer thickness, w, the built-in electric field can be determined by integrating Poisson's equation and applying boundary conditions at the surface and depletion thickness. For the condition $w > \lambda_L$, where w is the depletion layer thickness and λ_L is the optical penetration depth,then $E_B \approx E_{\max}$, and this yields

$$E_{\mathrm{THz}} \propto \pm \mu I_p \sqrt{N_i V_b / \epsilon_r}, \tag{5}$$

where V_b is the built-in potential, N_i is the impurity density, and ϵ_r is the dielectric constant of the material. A sign arises in eq. (5) depending on the carrier type, i.e. n- or p-type. Hence, from an observed signal one can deduce this.

B. Frequency-resolved optical gating

When working with ultra-short laser pulses we need some way of characterizing them, especially in terms of the pulse durations. One way to do this is to use an autocorrelation setup, which splits the pulse in two, with one part being sent on a delay stage. The two pulses then reconvene at an angle inside a crystal capable of second harmonic generation (SHG), which creates the autocorrelation signal itself. However, getting the pulse duration from an autocorrelation requires assumptions about the shape of the pulse. A way to remedy this is to use the frequency-resolved optical gating (FROG) technique [2]. The FROG technique, or at least the SHG FROG as we work with here, is in essence just an autocorrelation where the spectrum of the second harmonic light is recorded for each delay between the gate and probe pulse. The effect is that instead of yielding a direct autocorrelation (eq. 6)

$$A = \int_{-\infty}^{\infty} I(t) I(t-\tau) dt, \tag{6}$$

where A is the autocorrelation signal, t is the time, I is the intensity of the pulses and τ is the delay between the two pulses, then we get a so-called spectrogram (eq. 7) in the form of the intensity of the second harmonic light:

$$I_{\mathrm{FROG}}^{\mathrm{SHG}} = \left| \int_{-\infty}^{\infty} E(t) E(t-\tau) e^{-i\omega t} dt \right|^2, \tag{7}$$

where I_{SHG} is the intensity of the SHG signal, E is the electric field amplitude and ω is the frequency. In order to determine the pulse duration a phase-retrieval algorithm has to be run, which in our case was just done by software. Briefly, the idea is that the form above can be recast to the form of an already solved problem, called the "two-dimensional phase retrieval problem" [2], and then using the solutions for this problem the pulse duration can be determined.

C. Nonlinear fluorescence quenching

Quenching of fluorescence refers to any process reducing the intensity of fluorescence from a given material. A large variety of molecular interactions can result in such an effect, including collisions, excited-state reactions, and energy transfer [3]. Quenching processes may also arise from non-linear processes, hence called non-linear quenching, such as Auger recombination and exciton-exciton annihilation. In many practical applications such as scintillator detectors and LED, this is manifested as a loss of efficiency. Moreover, because the nonlinear quenching changes continuously and stochastically, the effect can be detrimental for high-performance devices [4]. In this setup the main interest is to simulate the material response to highly energetic radiation such as X-rays and γ-rays. To investigate nonlinear quenching high laser intensity is needed, which is achieved by tightly focusing a femtosecond pulse down to a beam waist on the micron scale. In the later section III C, the experimental methods employed to achieve this will be highlighted.

III. EXPERIMENTAL SETUPS

A. Terahertz generation from semiconductor surfaces using femtosecond lasers

The experimental setup for the THz generation is rather large, but a key part is how the overlap between the probe pulse and the THz signal is measured. This is a pump-probe setup, where the laser is separated into two pulses called a pump and a probe. After separation, the pump hits the sample, which depending on the material might result in THz generation. Then the pump is blocked by a thin sheet of Teflon, which still allows the THz pulse to pass through. Using a parabolic mirror, the THz signal is then focused on to a ZnTe crystal, which due to the electro-optic

effect causes a modulation in the crystal's index of refraction. The probe, which has a given polarization, is also focused onto the crystal such that it spatially overlaps with THz signal, which results in a change of its polarization depending on the temporal overlap with the THz pulse. The probe pulse is then split in two polarization components by a Wollaston prism, where each path is then measured by a photo detector. This then allows us to effectively scan over the THz pulse by varying the delay of the probe and monitoring the effect on the difference of the polarization components. In this way we can reconstruct the THz pulse, as we have made the difference of the polarization components proportional to it.

B. Frequency-resolved optical gating

The experimental setup for the FROG that was used has been sketched in fig. 1. Here a d-shaped mirror is used to split the incoming pulse in two, where one part, which we will call the probe pulse, is sent into a delay stage, and the other part then functions as the gate pulse. The two pulses then meet at the mirror furthest to the left (marked A on figure 1) and after propagating a bit further they are focused into a BBO crystal for SHG. This results in three different SHG signals, which can be understood by considering energy and momentum conservation for individual photons. From momentum and energy conservation we have either

$$\boldsymbol{k_{SHG}} = 2\boldsymbol{k_1}, \quad \boldsymbol{k_{SHG}} = 2\boldsymbol{k_2} \text{ or } \boldsymbol{k_{SHG}} = \boldsymbol{k_1} + \boldsymbol{k_2} \quad (8)$$

where $\boldsymbol{k_{SHG}}$ is the momentum vector of an SHG signal photon, and $\boldsymbol{k_1}$ and $\boldsymbol{k_2}$ are the momentum vectors of a photon from each of the two pulses. If the two pulses don't temporally overlap then we only have the possibility of generating the SHG photon by combining two photons from the same pulse. This results in the upper and lower signals shown on figure 1 as the momentum conservation yields either $\boldsymbol{k_{SHG}} = 2\boldsymbol{k_1}$ or $\boldsymbol{k_{SHG}} = 2\boldsymbol{k_2}$. As we can see, these SHG photons will move in the same direction as their parent pulse, which means they will come out with an angle relative to the central axis of the SHG crystal. If the two pulses do temporally overlap, then we can also generate the SHG photon by combining one photon from each pulse such that $\boldsymbol{k_{SHG}} = \boldsymbol{k_1} + \boldsymbol{k_2}$. This results in the middle SHG signal seen on figure 1 as the components of $\boldsymbol{k_1}$ and $\boldsymbol{k_2}$ that are orthogonal to the to the central axis of the SHG crystal cancel each other out.

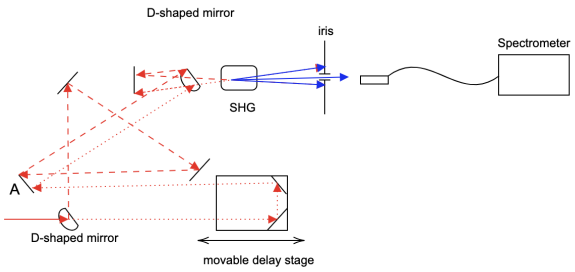

Figure 1: Sketch of the FROG setup. The dotted and dashed lines indicate the two different beam paths, and their overlap is indicated by a line that is both dotted and dashed.

It is this middle signal, which is isolated by use of an iris, that is sent into a spectrometer. A spectrum of the second harmonic light is then recorded for each position of the delay stage and from these spectra the phase retrieval algorithm, which has already been implemented in a python program in the lab, can extract the pulse duration.

1. *Chirped Pulse Amplification*

To examine the effects of the laser pulse duration on the FROG trace we varied the pulse compression of the setup. Pulse compression here refers to the final step in a chirped pulse amplification (CPA) scheme, which is a common method to amplify ultrashort laser pulses. As ultrashort laser pulses can reach high peak intensities sending these through a solid gain medium can lead to material damage due to self-focusing effects. In order to avoid this one can place a grating pair introducing a large chirp on the ultrashort laser pulse through their dispersion, thus increasing the pulse duration. The now stretched pulse can then be safely sent into the gain medium as the longer pulse duration yields a lower peak intensity. Afterwards, the amplified and stretched pulse can be compressed by another grating pair resulting in a laser pulse with a similar duration to the initial pulse, but now it has been amplified. It is this final stage that we intentionally worsen (that is, reduce the amount of compression) in one of the FROG traces in order to compare two FROG traces of pulses with different durations.

C. Nonlinear fluorescence quenching

In this experiment, which has been sketched in figure 2, the femtosecond pulse is also generated by

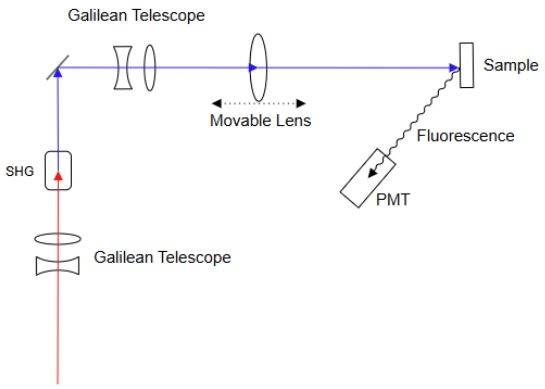

Figure 2: Sketch of the fluorescence quenching setup. In the measurements of the beam profile the sample was replaced with a beam profiler.

a Ti:Sapphire laser. As highlighted in Section II C, this experiment concerns itself with simulation of high photonic energies. For that reason second-harmonic generation is performed to double the photonic energy. Because only the second-harmonic is used in this experiment, a high conversion efficiency is wanted. Because the intensity of the second-harmonic is related to the intensity, I, as

$$I(2\omega) \propto \omega^2 \chi^{(2)} L^2 I(\omega)^2, \tag{9}$$

where ω is the frequency, $\chi^{(2)}$ is the nonlinear susceptibility and L is the length of the SHG medium, a high conversion factor can be achieved by using high intensities [5]. To achieve this, the beam waist is tightly focused using a Galilean telescope. However, because we later want to narrow the waist down to the μm-scale, it is important to consider the implications of this. From Gaussian propagation the waist follows the profile

$$w(z) = w_0 \sqrt{1 + \left(\frac{\lambda z}{\pi w_i^2}\right)^2}, \tag{10}$$

where $w(z)$ is the beam radius at position z, w_0 is the beam waist, λ is the wavelength and w_i is the initial beam radius. Using the $ABCD$-matrix approach, the focusing of the beam can be considered. By assuming that $w_{\text{final}} \gg w_{\text{initial}}$, that is, a strong focusing is applied, the final beam waist, w_f is given as

$$w_f \simeq \frac{f\lambda}{\pi w_i}. \tag{11}$$

Essentially, this means that because $w_f \propto 1/w_i$, it is easier to produce a very tightly focused beam from an initially larger waist size [6]. For this reason, after the SHG a Galilean telescope is used to expand the beam waist. To achieve a very tightly focused beam, a strong focusing lens is placed onto a rail, where the position of the lens can be electronically controlled, and the beam is initially dumped onto a scanning-slit beamprofiler to determine the waist. When the beam is not very focused, the beamprofiler can not reliably determine the waist, and therefore this has to be done manually by exporting the data directly. By moving the lens back and forth on the rails, the waist at the position of the beamprofiler changes, and doing this for all positions the beam waist can be characterized at all positions. By knowing the waist at all positions, it is possible to relate this to the peak fluence. By placing a sample material at the position of the beamprofiler, the resulting fluorescence of the sample can be measured.

IV. RESULTS

A. Terahertz generation from semiconductor surfaces using femtosecond lasers

As seen in fig. 3, the THz generation from an InAs sample and bulk Ge sample was examined. In fig. 3a we see the signal from InAs, and in fig. 3b the Fourier transform of that signal. As expected, we see that the signal contains frequencies in the THz regime. Looking at figure fig. 3a we can also see another pulse located at around 5.6 ps. This is a part of the THz pulse which experienced one round trip inside the teflon block and is called the first reflection. Using the delay between the initially transmitted THz signal and the first reflection we estimated the thickness of the teflon block to be 0.23 ± 0.05 mm. In fig. 3c we see the signal resulting from the illumination of the bulk Ge sample and the Fourier transform of that signal can be seen in fig. 3d. Here, we also seem to see a THz generation signal, but it turned out to not actually be from the bulk Ge, which is further discussed in section V A.

Moreover, because of the detection setup used, the observed signal is directly proportional to the electric field of the THz radiation, i.e. eq. (5).

B. Frequency-resolved optical gating

Working with the FROG, we made two traces of the fs-laser. One trace, where the pulse compression was

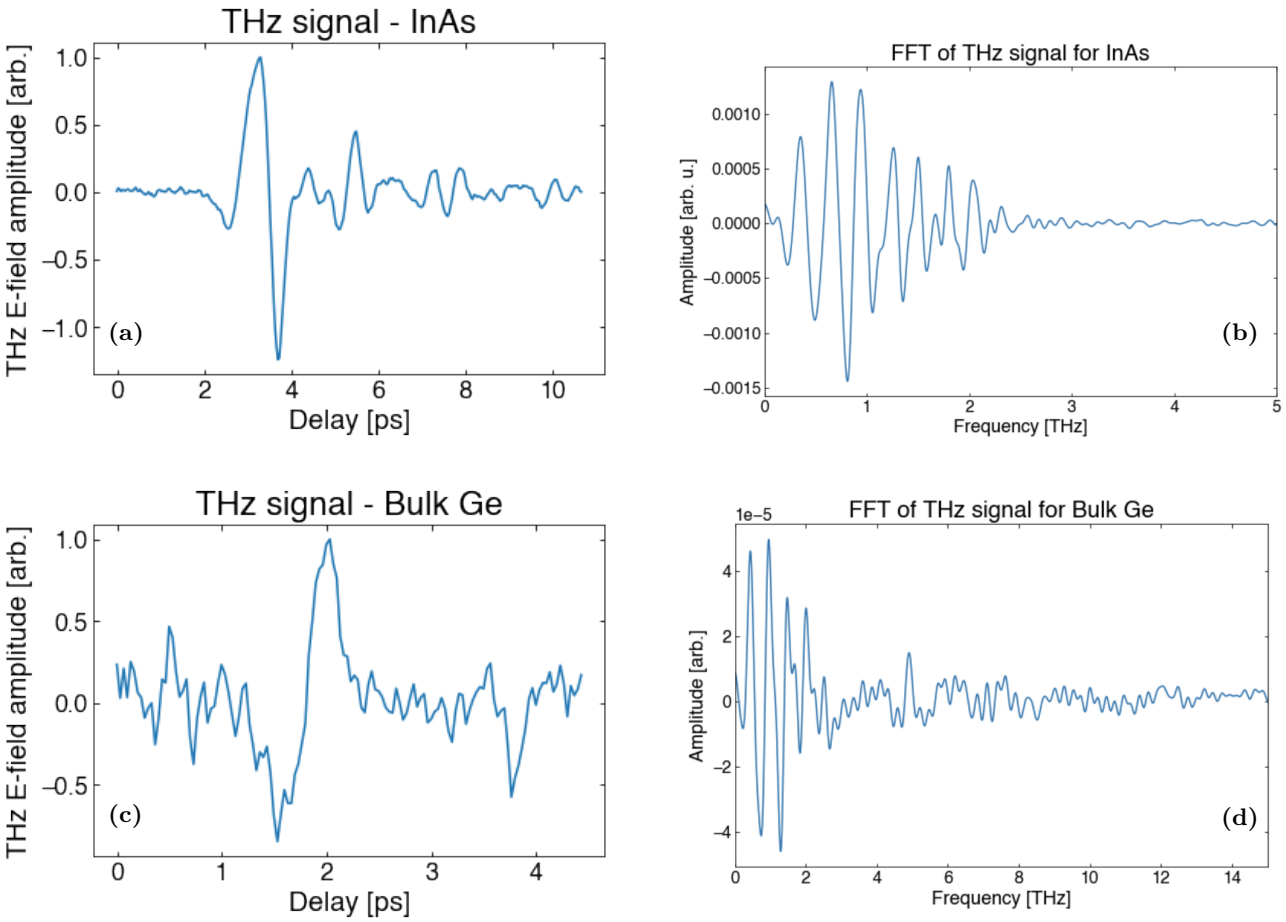

Figure 3: Resulting THz signals and their Fourier transforms, when illuminating the known THz radiation source (a, b) InAs and (c, d) bulk Ge. As observed in (b, d) both samples clearly produce THz radiation, although less cleanly for the bulk Ge.

not altered from the setup standard, and another trace where the pulse compression was intentionally worsened in order to see the effects on the FROG trace. The results can be seen in fig. 4, where we see that the pulse with the intentionally worsened compression is longer that the pulse with non-altered compression as one would expect.

C. Nonlinear fluorescence quenching

As discussed in section III C, the beam waist has to be characterized at the various positions on the rails (denoted *motor position*). Ordinarily, one would use eq. (10), however due to beams typically deviating slightly from the normal Gaussian profile, a parameter M^2 is added, denoting the *beam quality factor*, which for an ideal Gaussian beam would be equal to 1. Hence, our fitting function is

$$w(z) = w_0\sqrt{1+\left(M^2\cdot\frac{\lambda(z-z_0)}{\pi w_i^2}\right)^2}, \qquad (12)$$

also allowing for a displacement along the z-axis via the z_0 parameter. In order to tightly focus the waist of the beam, a Galilean telescope expands the beam prior to the final focusing lens as discussed previously. By using the beamprofiler, the beam waist can be characterized at the various motor positions. In fig. 5 the resulting difference can be seen, and in table I the resulting fit coefficients can be seen. As seen in fig. 5 and table I, by expanding the initial beam waist by a factor of about 5 using the Galilean telescope, the beam waist minimum becomes smaller by a factor of 7. Moreover, it seems that the beam quality factor also slightly decreases, but this may also be due to more careful alignment. Far away from the waist minimum the fit of especially fig. 5b deviates from

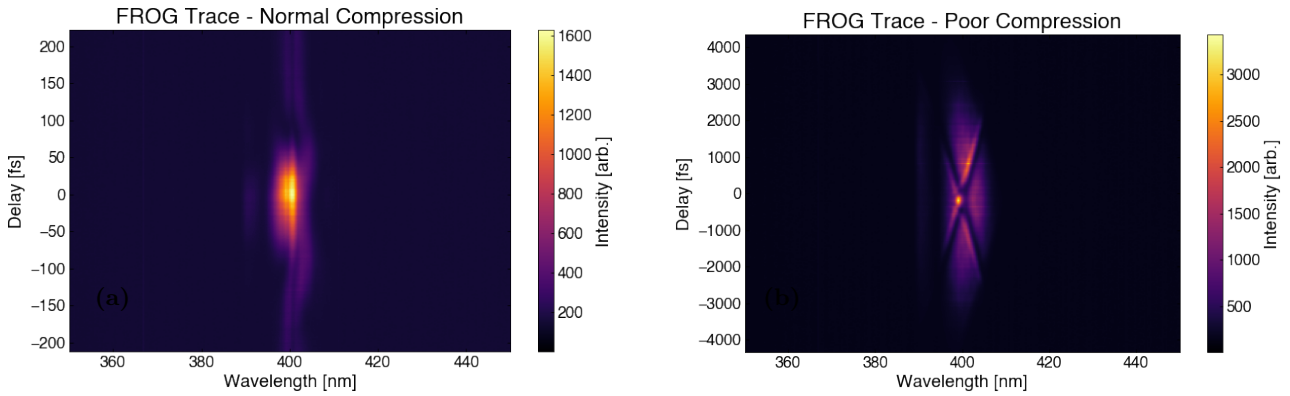

Figure 4: The two FROG traces for normal pulse compression (left) and intentionally worsened pulse compression (right). Looking at the vertical axis we clearly see that the pulse with worsened compression has been stretched in time.

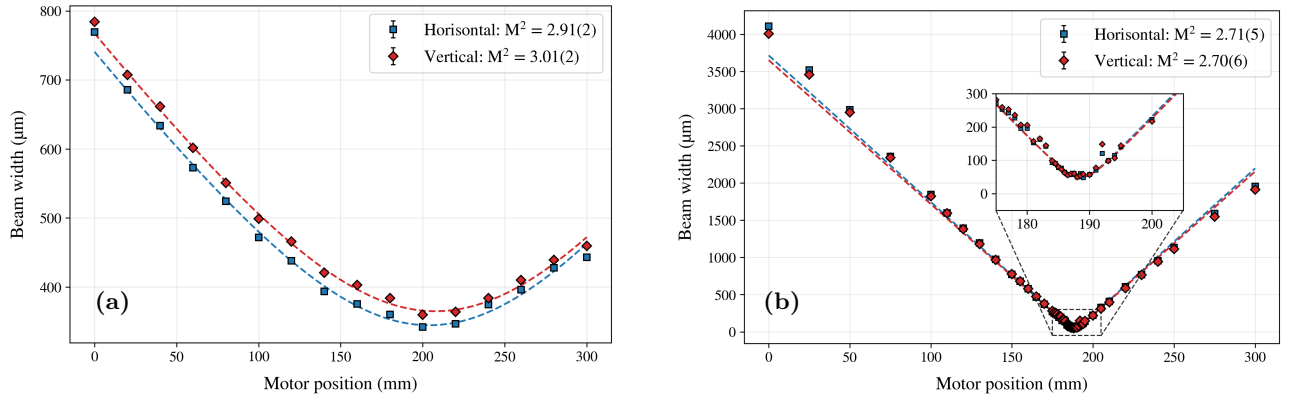

Figure 5: Measurements of the Gaussian beam profile of (a) without initial expanding of the beam using a Galilean telescope and (b) with initial expanding. As observed on the limits of the vertical axis, the beam is initially 5 times broader. By doing this, it is possible to focus it down from (a) $w_0 \sim 350(3)$ μm to (b) $w_0 = 49(2)$ μm.

(a)

	x	y
w_0 (μm)	343(3)	364(3)
M^2	2.92(2)	3.02(2)
z_0 (mm)	204(2)	208(2)

(b)

	x	y
w_0 (μm)	49(2)	49(2)
M^2	2.71(5)	2.70(6)
z_0 (mm)	188.5(1)	188.6(1)

Table I: Fitting results of eq. (12) for the vertical and horizontal beam profile for (a) without initial beam expansion and (b) with.

the data, which is not directly observed for fig. 5a. This is expected to be due to poor collimation of the beam, explaining the lack of deviation at the waist minimum.

By directing the fs-pulse onto a sample material instead of the beamprofiler, the fluorescence of the sample can be measured with photo-multiplier-tubes. Relating the beam waists to the peak fluence can be done using

$$I_{\text{fluence}} \propto \frac{1}{w_x(z) \cdot w_y(z)}. \tag{13}$$

Measuring the total light yield from the PMTs for the various motor positions (and fluences) fig. 6 was made. As observed, by tightly focusing the beam and increasing the peak fluence the PMT signal significantly drops by 99% around z_0. Clearly this shows that in the sample a quenching process occurs, which manifests itself as a loss in total light yield. Without any nonlinear quenching effects, the PMT signal would be expected to remain constant.

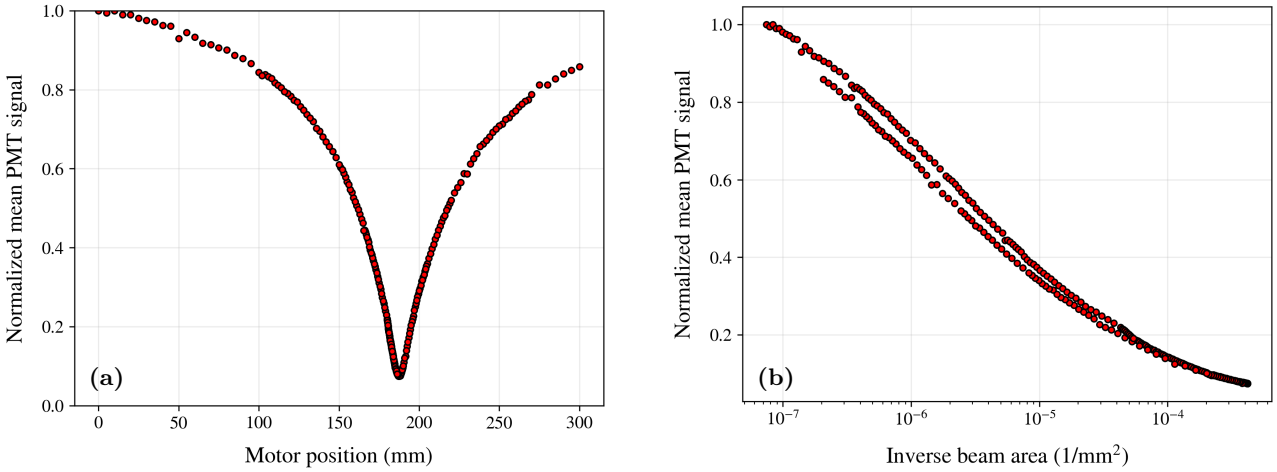

Figure 6: Measurement of total light yield from CdSe/CdS core/crown nanoplates fluorescence at various motor positions, in (a) characterized by the motor position, and (b) with peak fluence through eq. (13). As seen, quenching occurs which decreases the light yield from the PMT signal.

V. DISCUSSION

A. Terahertz generation from semiconductor surfaces using femtosecond lasers

As seen in section IV A, the InAs sample produced a clean THz radiation signal as expected. In regards to the bulk Ge THz signal, it was later found that the InAs sample and the bulk Ge sample had been placed too close to each other. This meant that we had accidentally also illuminated the InAs sample together with the bulk Ge sample, hence the THz radiation again stems from InAs. Furthermore, we also observed some fast oscillations in the FFT's of the THz signals, which we can't account for.

B. Frequency-resolved optical gating

The results of the FROG traces in section IV B follows closely what was expected. Namely, we saw that the worsened compression shows in the FROG trace, where that pulse was broader in time, compared to the pulse with proper compression.

C. Nonlinear fluorescence quenching

In section IV C, we saw that we were able to bring the laser to a much narrower focus by initially expanding it using a Galilean telescope. This nicely follows the expected relation from eq. (11). With the measurements of nonlinear quenching, we clearly see a dip in the PMT signal around the focus of the beam as expected. We can also see in both fig. 6a and b that the response before and after z_0 is asymmetric. This could be due to damage to the material that alters the response after passing the focus or from the asymmetrical beam profile as can be seen on figure 5b.

VI. CONCLUSION

In this project we have worked with a Ti:Sapphire fs-laser in relation to THz generation and nonlinear fluorescence quenching. Here, we saw THz generation from InAs after illumination by a fs laser, worked with applications of Gaussian beam optics to manipulate the focus of the laser, and saw nonlinear fluorescence quenching in a prospective detector material. Furthermore, we have also worked with a FROG setup and used it to see the effects of pulse compression through the FROG traces. In conclusion, the project was a well-rounded tour of fs-laser principles and applications.

[1] Masayoshi Tonouchi. Simplified formulas for the generation of terahertz waves from semiconductor surfaces excited with a femtosecond laser. *Journal of*

Applied Physics, 127(24):245703, 06 2020. ISSN 0021-8979. doi:10.1063/5.0005623. URL https://doi.org/10.1063/5.0005623.

[2] Rick Trebino, Kenneth W. DeLong, David N. Fittinghoff, John N. Sweetser, Marco A. Krumbügel, Bruce A. Richman, and Daniel J. Kane. Measuring ultrashort laser pulses in the time-frequency domain using frequency-resolved optical gating. *Review of Scientific Instruments*, 68(9):3277–3295, 09 1997. ISSN 0034-6748. doi:10.1063/1.1148286. URL https://doi.org/10.1063/1.1148286.

[3] Joseph R. Lakowicz. *Principles of Fluorescence Spectroscopy*. Springer, New York, NY, 3 edition, 2006. ISBN 978-0-387-31278-1. doi:10.1007/978-0-387-46312-4. Hardcover. Also available as Softcover (Published: 30 April 2017) and eBook (Published: 05 December 2007). Total Pages: XXVI, 954. Topics include Mass Spectrometry, Analytical Chemistry, Biological and Medical Physics, Biophysics, Biochemistry, general, Biotechnology, Physical Chemistry.

[4] Joel Q. Grim, K. B. Ucer, A. Burger, P. Bhattacharya, E. Tupitsyn, E. Rowe, V. M. Buliga, L. Trefilova, A. Gektin, G. A. Bizarri, W. W. Moses, and R. T. Williams. Nonlinear quenching of densely excited states in wide-gap solids. *Phys. Rev. B*, 87:125117, Mar 2013. doi:10.1103/PhysRevB.87.125117.

[5] P. W. Milonni and J. H. Eberly. *Laser Physics*. John Wiley & Sons, Incorporated, 2010.

[6] Frank L. Pedrotti, Leno M. Pedrotti, and Leno S. Pedrotti. *Introduction to Optics*. Cambridge University Press, 3rd ed. edition, 2018. ISBN 978-1-108-42826-2.